

# Automated Scoring of Acid-Fast Bacteria by Fluorescent Smear Microscopy

## Author

Wendy Goodrich  
Agilent Technologies, Inc.

## Abstract

Bacterial strains in the genus *Mycobacterium* have a unique cell wall architecture that can be used to differentiate them using acid-fast staining assays, hence their description as acid-fast bacteria (AFB). Some human and livestock diseases are caused by AFB, and microscopy methods are used as part of a screening process to identify presumptive AFB positive samples of those potentially exposed. These samples are generally scored within categories described by the number of AFB counts per field of view (FOV) over multiple FOV dependent on magnification. Performed manually, this process can result in over- or undercounting due to operator visual fatigue or variability of identification between operators. An automated microscopy and analysis protocol is described in this application note as an alternative method for AFB scoring that could increase accuracy and reproducibility over manual scoring.

## Introduction

Acid-fast bacteria (AFB) share a property derived from the composition of an outer membrane surrounding their cell wall that contains a notably large percentage (40 to 60%) of mycolic acids. These long chain fatty acids form a thick lipid layer that confers a resistance to acid alcohol decolorizers during differential staining techniques. Two common AFB staining procedures that exploit this property use the fluorescent stains Auramine O, and Auramine O-rhodamine B. These fluorophores are highly lipophilic and thus show a strong affinity for AFB resulting in well-defined bright staining against nonspecific background under a fluorescence microscope. Some limitations of these staining methods include the inability to identify individual strains of mycobacteria and carcinogenic properties of the dyes, however fluorescent staining methods of AFB are easy to perform, cost effective, and produce rapid results. As such, they have been adopted into workflows that use fluorescent smear microscopy to screen for acid-fast bacteria, most notably as part of the diagnostic screening protocol for the pathogenic strain *Mycobacterium tuberculosis*, the cause of the disease *tuberculosis* (TB).<sup>1</sup> Diagnostic screening protocols classify a total AFB score that is magnification dependent and obtained by scanning and counting multiple fields of view (FOV) on a standard 2 × 1 cm sample smear, the number of FOV dependent on objective magnification.<sup>2,3</sup>

Table 1 describes typical criteria for assessing AFB assuming a total magnification of the objective and a compensating ocular present on common manual microscopes.


*Mycobacterium tuberculosis* typically presents as rod shaped objects 1 to 10 μm in length by 0.2 to 0.6 μm wide, and classically, but not always, curved, bent, granular, or beaded. A standard positive smear can contain a highly confluent mix of bacterial presentation, including clusters and swollen cells.<sup>4</sup> Because of their small size, variation in morphology, and the required number of individual sample areas to count, manual AFB scoring can be tedious and prone to error. Operator visual fatigue has been cited as a reason to limit microscopist examination in AFB scoring.<sup>5</sup> In part to help alleviate this problem, the World Health Organization validated and recommended LED-based microscopy for TB fluorescent smear screening in 2011.<sup>5</sup>

Quality control slides are often used as positive and negative controls for each run of specimen smear testing for a number of reasons, including as a means to establish and confirm correct functioning and settings of a microscope.<sup>6</sup> As such, QC smears containing a mix of acid-fast positive and negative bacteria, including deactivated *M. tuberculosis* H37Ra, were


**Table 1.** An example of criteria for screening AFB using fluorescent smear microscopy.<sup>2</sup>

Magnification <sup>b</sup>	Number of Fields
200x	30
250x	30
400x	55
450x	70

<sup>a</sup> The minimum number of fields to examine before reporting a smear as negative for acid-fast organisms

<sup>b</sup> This final magnification represents the objective lens magnification multiplied by the eyepiece magnification 

Report	Number of AFB Observed*	
	200x,250x	400x,450x
No AFB seen	0	0
Doubtful: repeat	1-2/30F	1-2/70F
1+	1-9/10F	2-18/50F
2+	1-9/F	4-36/10F
3+	10-90/F	4-36/F
4+	>90/F	>36/F

\* number of acid-fast bacilli observed per microscopic field 

deemed a good model to develop an automated imaging and analysis protocol for AFB screening using fluorescent channels of an inverted digital widefield microscope. The automated microscope used was controlled by software defined with a montage and stitching algorithm, enabling the ability to image and analyze multiple adjacent areas of a sample resulting in a final AFB score. This automated approach could be used as a means to decrease microscopist visual fatigue, and increase examination throughput, accuracy, and reproducibility by offering an alternative to manual scoring. As with all screening methods, it is assumed laboratories would validate and establish their own optimal configuration and settings according to individual protocols and expertise. This is particularly important when converting FOV area from a manual microscope to a digital

microscope without ocular compensation. Figure 1 compares representative image dimensions from the automated digital microscope used in this application note to a theoretical configuration for a manual microscope assuming a 2 × 1 cm (L × W) smear size.

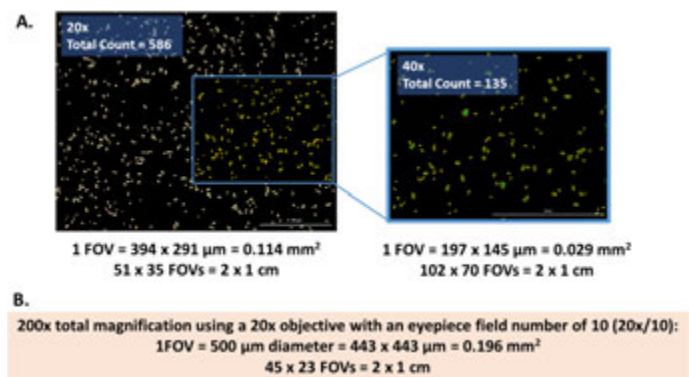


**Figure 1.** (A) Representative results of one field of view using a 20x and 40x objective obtained from the digital microscope used for the automated AFB screening method described by this document compared to those of a theoretical nondigital microscope with ocular compensation (B).

## Method

### Staining assay

Positive and negative smears on BBL AFB Slides (BD Part number 231391) were fixed in methanol as described previously.<sup>7,8</sup> Fixed, air dried smears were stained according to the procedure of the BD TB Fluorescent Stain Kit T (part number 212521) with the exception that smears were stained in a pool of reagent rather than stained by streaming reagent over the slide. Reagents were washed using a gentle stream of deionized water that had been treated in an autoclave for 25 minutes, allowed to cool, and then filtered through a 0.2 μm membrane into a sterile 500 mL wash bottle. Smears were then allowed to air dry before mounting in a tris-buffered glycerin (pH 9.0 ±0.5) and 0.1% sodium azide solution, or with Shandon Shandon-Mount (Thermo Fisher Scientific part number 1900331) and cover slipped. The slides were either imaged immediately (glycerin mounted), or following an overnight cure in the dark at room temperature (Shandon mounting medium). There were some advantages to the Shandon medium compared to the glycerin: the Shandon hard cure was more amenable to inverted imaging allowing slightly better resolution through a coverslip rather than through the microscopy slide; preservation of the fluorescent signal over time; and the ability to store samples long term for record keeping or re-imaging if required. A summary of the staining assay is shown by Figure 2.

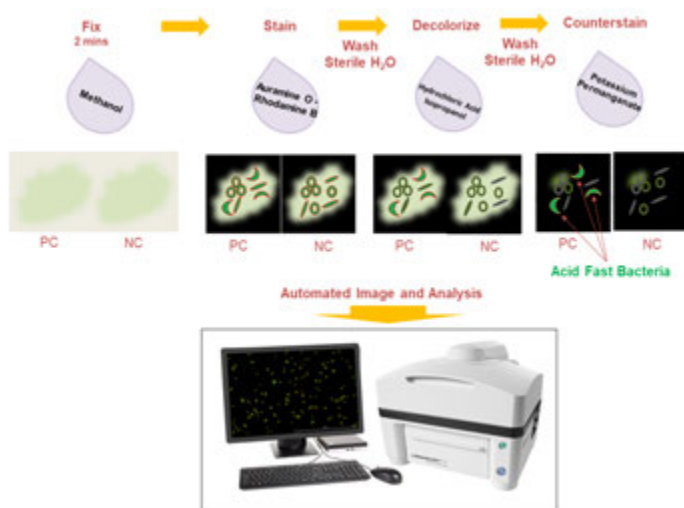


**Figure 2.** Overview of the staining assay workflow used to demonstrate automated AFB scoring. AFB resist decolorization by acid alcohol and therefore retain the primary stain. They can then be differentiated and enumerated using a fluorescence microscope, as demonstrated by this application note using an Agilent BioTek Lionheart FX automated microscope and Agilent BioTek Gen5 microplate reader and imager software.

### Imaging assay

Slides were loaded into an Agilent BioTek slide adapter (part number 1220548) or an Agilent BioTek 4 slide holder (part number 1650516) in both a coverslip down (Shandon) and/or coverslip up (glycerin) configuration (data not shown). An Agilent BioTek Lionheart FX automated microscope controlled by Agilent BioTek Gen5 Image Prime software was used to image slides using 20x (part number 1220517), 40x (part number 1220544), and/or 60x (part number 1220545) objectives with correction collar settings of 0.17 (coverslip down) or 1.00 (coverslip up). A 6 × 5 montage of 30 images was acquired of auramine staining with a GFP filter cube (part number 1225101) equipped with a 465 nm LED cube (part number 1225001). Rhodamine staining was imaged using an RFP filter cube (part number 1225103) equipped with a 523 nm LED cube (part number 1225003). Optimal exposure settings were determined for each objective using a positive control smear and then applied to all images for both positive and negative controls. Images were background corrected using image preprocessing settings of a rolling ball size of 2 μm for auramine and 5 μm for rhodamine, both with fine results and a smoothing factor of 2. Following image preprocessing, montages were stitched on the GFP channel using a linear blend method and no image downsizing. A primary mask was defined on auramine stained objects (GFP channel) with a size from 1 to 13 μm and a signal threshold of 9,108. A secondary mask was defined on RFP within a minimally expanded (1 × 10<sup>-7</sup>) perimeter area of the

primary mask to define a threshold above background of 1,472. To calculate the percent of total GFP object counts that were also RFP positive, a subpopulation was defined on objects greater than or equal to the lowest RFP signal intensity from the secondary mask analysis. Masking size and signal thresholds are dependent on the image background correction option. Due to the staining intensity and tendency of AFB to present as individual, clusters, and/or overlapped cells, image background correction, and masking thresholds can be customized according to protocol and staining technique. Representative results for slides imaged coverslip down and mounted in cured Shandon are shown by Figures 4 to 9.

## Results and discussion

The QC AFB positive and negative controls come smeared within a stamped circular area 15 mm in diameter, and the defined montage size was designed to be representative within that area to demonstrate proof of principle. In the Agilent BioTek Gen5 software, up to 2,000 images can be

acquired in a single montage, depending on the objective used. Figure 3 highlights a montage designed for two objective magnifications, and the montage positioning values that can be adjusted depending on the size and location of the smear (shown in light green). Note that only one imaging step is required to image a 2 x 1 cm smear at 20x ( $51 \times 35 = 1,785$  images), whereas at 40x ( $102 \times 70 = 7,140$  images) requires more than one montage defined by multiple imaging steps in sequence to image the same smear area (Figure 3, blue arrows). Further, the montage definition assumes that smears are of identical size and location for each sample. Two workarounds for this could be to always mark the same area on a sample slide for smearing, or to adjust the montage area using the horizontal and vertical positioning values (Figure 3, pink arrow). These can be determined either by physically measuring where the smear is on the slide and converting to micron units ( $\mu\text{m}$ ), or by using the brightfield channel to obtain position values by scanning the slide (Figure 3, green arrow). Once the montage area is defined, the images are taken by moving left to right equidistant from the center of the offset.

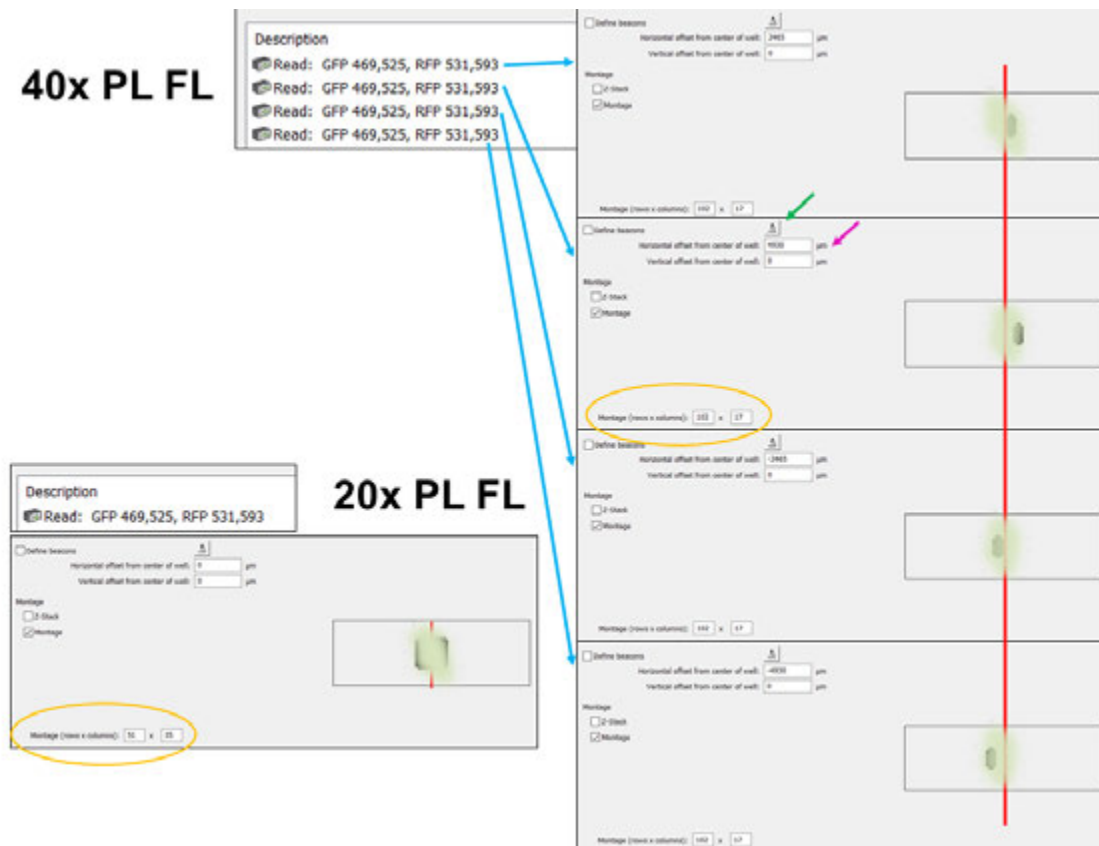


**Figure 3.** The montage imaging area (black) is dependent on objective magnification and position of the region of interest. This example assumes that a 2x1 cm smear (light green cloud) is in the geographic middle of a standard microscopy slide.

Figure 4 illustrates stitched images from 6 × 5 montages of the positive (4A) and negative (4B) controls. It is evident that the positive control contains a large number of AFB, while the negative control does not. Following acquisition, images are background corrected as shown for a single tile, and then stitched into a final montage. Both controls are captured, preprocessed, and stitched with the same settings. It was found that preprocessing before stitching could result in some tiles being unresolved due to a lack of signal in the negative control (data not shown). Preprocessing after stitching resulted in lower threshold values, but cell counts remained relatively constant. If unresolved errors occur during stitching, it should be done before background correction.

Overlap between adjacent individual montage tiles are rendered as a single area during stitching, removing

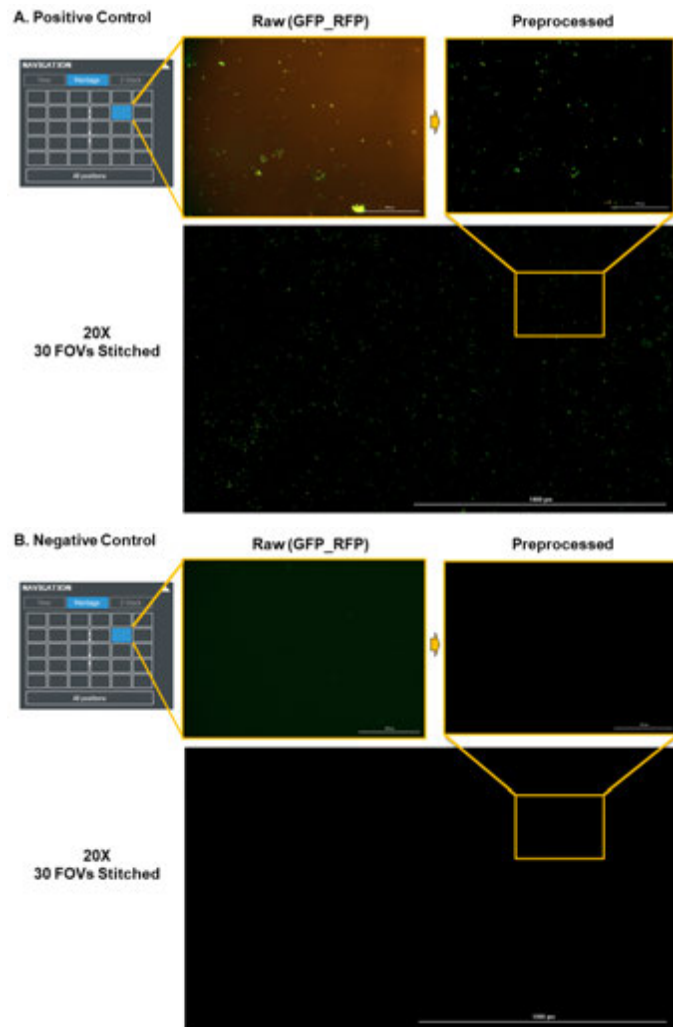


**Figure 4.** A single tile view of the positive control (A) and negative control (B) within a final stitched image containing 30 FOVs using a 20x microscope objective.

the possibility of duplicate object counting in the final montage (Figure 5). The overlap value can be customized if required. If analyzing cell counts on individual tiles of a montage rather than the stitched image, however, the overlap area between adjacent images (X and Y) should be factored into final cell counts. Importantly, because of the small size of AFB, the image downsize option within the stitching interface should be turned off so as to retain full resolution of images for maximum stitching accuracy.

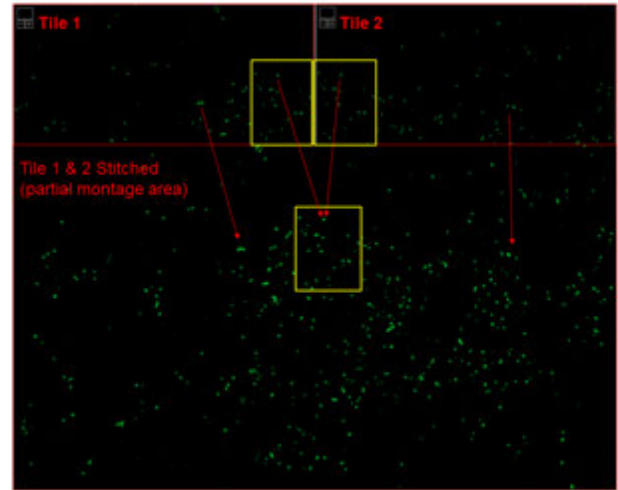


**Figure 5.** Top: individual adjacent montage tiles; Bottom: portion of the stitched image showing the two adjacent tiles. Red arrows show line up between individual tiles and the stitched image. Yellow areas show where image overlap between two adjacent tiles becomes a single area in the stitched image.

Counting AFB was performed using a primary mask threshold on auramine staining with the GFP fluorescence channel. Secondary masking was done on rhodamine staining with the RFP fluorescence channel to determine dual stained objects. Figure 6A shows a typical image and counting of AFB using both fluorescence channels. Figure 6B illustrates how counted objects can be characterized according to a number of metrics using scatter plots and histograms to supplement AFB scores with data on object subpopulations, morphology profiles, or staining patterns, for example. The histogram shown illustrates that 80.6% of the total objects of the smear were dual stained positive, and that those objects have a higher mean RFP signal as a result of the subpopulation analysis.

AFB counts and scoring based on the criteria expressed in Table 1 are shown for four separate positive and negative QC smears in Figure 7. On the left are the total auramine and dual stained counts from 6 × 5 stitched montages of four control smears, and on the right are the mean counts per field of view, calculated by dividing the total stitched counts by the number of fields of view of the montage (30).



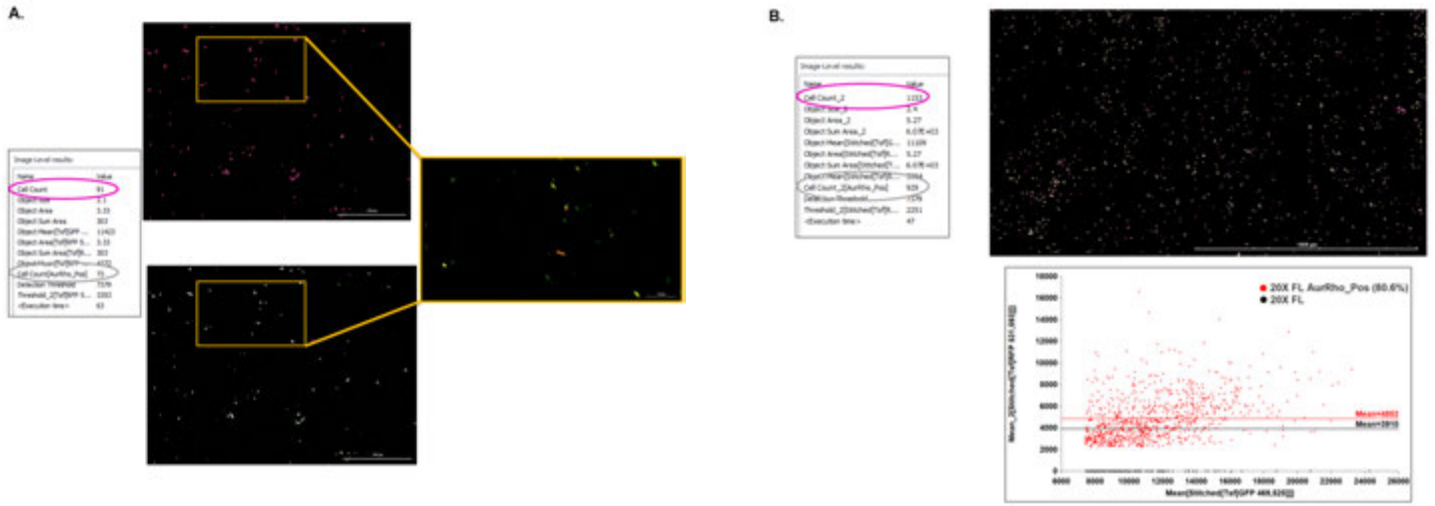


**Figure 6.** (A) As shown on a single image, primary masking on auramine at 20x yields total counts (purple) and secondary masking and subpopulation analysis identifies and counts objects that are also rhodamine positive (white/light grey). A zoom on one area is shown without masking (right). (B) The distribution of total counted objects (black dots) and the percent of total objects that are both auramine and rhodamine positive (red dots) is shown by a scatter plot on the results of the montage analysis.

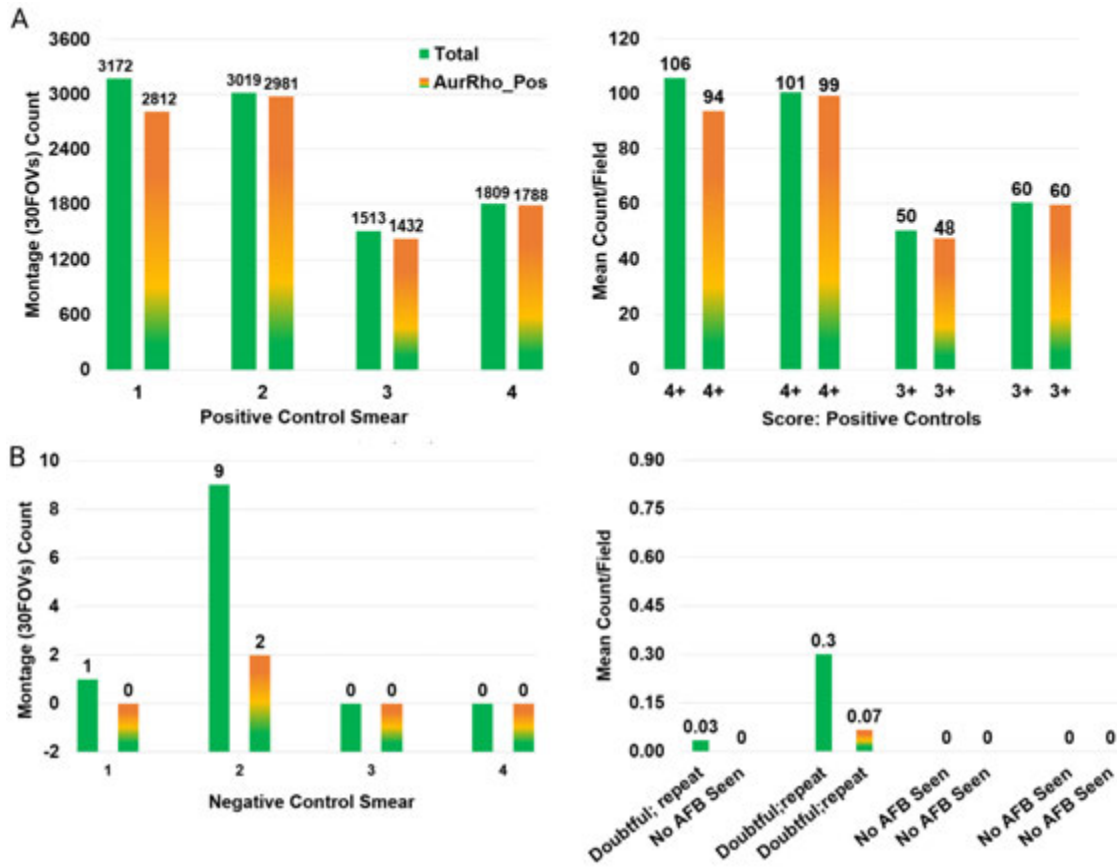


**Figure 7.** Final scores of montage images for representative positive (A) and negative (B) smears using the criteria from Table 1.

One probable explanation for the difference in counts between auramine and dual stained objects is shown by Figure 8. Rhodamine presents a lower and more variable staining intensity than auramine, even though the background correction defined during preprocessing was higher for rhodamine than auramine to retain more signal. Because of the decreased signal recognition of rhodamine, some objects were rendered below the defined background threshold during subpopulation analysis, and were excluded by the secondary masking criteria of auramine positive objects.

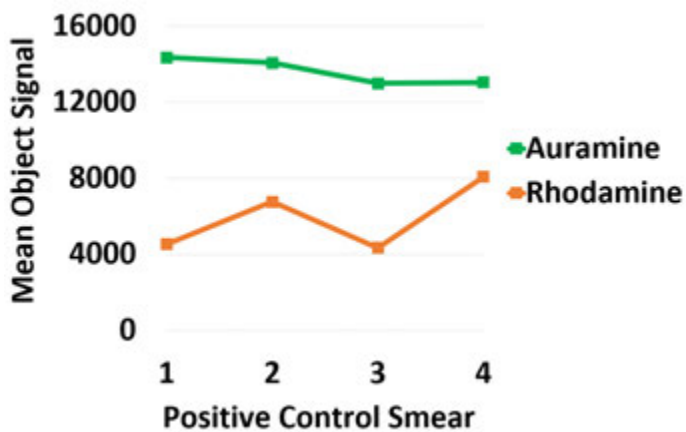


**Figure 8.** As shown for montage results of multiple smears, rhodamine exhibits lower and more variable staining intensity than auramine.

A nonspecific staining pattern of rhodamine was also revealed during masking, shown by some objects that presented with rhodamine staining and AFB morphology that were not auramine positive. This is illustrated using a higher resolution objective at 60x magnification by Figure 9. Purple objects in the image on the right are auramine/rhodamine positive objects detected from the image on the left. Although there is no indiscriminate auramine staining presented on the right, there are a number of rhodamine artifacts shown by the arrows. The QC positive control smear contains two strains that are not acid-fast, *Staphylococcus aureus* and *Escherichia coli*. In addition to being lipophilic, rhodamine intercalates cellular DNA more generally, so rhodamine staining of these non-AFB strains may be expected to be more prevalent and could be a cause of the nonspecific staining pattern of the dye. Upon analysis of a representative negative control QC smear, containing only *S. aureus* and *E. coli*, three Auramine objects were masked, one of which was dual staining positive. However, using the rhodamine channel as the primary mask, 90 objects were detected that were rhodamine positive and auramine negative. The incidence of this staining pattern was only partially resolved by decreasing the rolling ball size on rhodamine to further flatten the background (data not shown). This tendency

towards nonspecific staining of rhodamine suggests that auramine is a more reliable primary stain for masking total AFB object counts, but that auramine positive objects that are rhodamine negative are likely to be AFB indefinite.

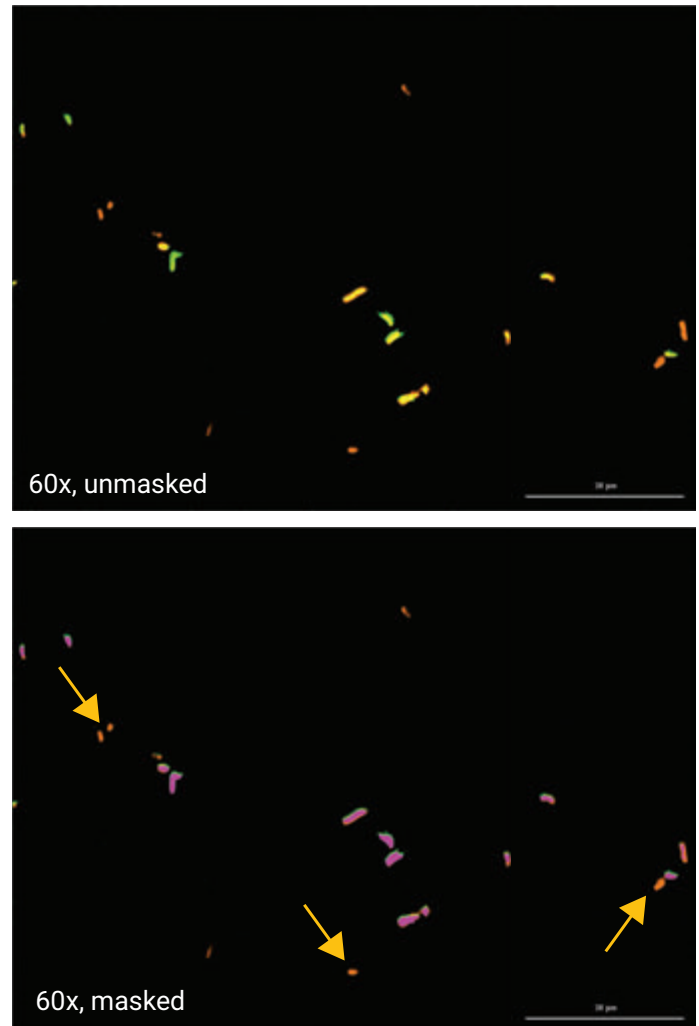


**Figure 9.** At higher resolution, a nonspecific staining pattern of rhodamine can be observed from artifacts not masked as auramine positive (arrows).

## Conclusion

Fluorescent staining of AFB positive and negative QC smears was used as a model to develop an automated microscopy and analysis procedure that could be applied to a typical AFB enumeration workflow. This method could relieve visual fatigue and/or operator variability that may occur from manual scoring. Automated preprocessing steps increased signal contrast to improve sensitivity of object recognition. Some artifacts may be included in analysis regardless of preprocessing, although with aggressive background correction larger artifacts will be excluded. Conversely, some

AFB positive cells that resolve as weakly stained because they are just outside of the optimal focal height may be excluded from analysis. Montage and stitching were used to capture multiple fields of view to expand object acquisition over a large smear area, and can be customized according to application protocol. Based on the small size of AFB it is recommended to turn off the stitching image downsize percent to retain the highest resolution of objects within the final montage. Primary masking resulted in an automatic count of auramine stained AFB objects. Secondary masking and subpopulation analysis on rhodamine was used to count objects that were auramine-rhodamine positive and can be shown as a percent distribution using a scatter plot. Threshold values for counting should be determined on results of each channel using positive controls, and the same values then used consistently on negative controls and samples. Dual staining is advantageous to help increase confidence and accuracy in object counts, but of note, in the experiments done here, rhodamine stained with less intensity and more variability than auramine, predisposing auramine as a recommended primary stain for masking total object counts in AFB dual staining fluorescence screening assays. Higher resolution objectives can be employed on regions of interest with lower object counts, indeterminate object presentation, or to confirm morphology if required.

Additional standard features of the Agilent BioTek Lionheart FX automated microscope that enable expanded options for acid-fast smear microscopy include a 6-objective turret that fits a range of objectives from 2.5x up to 100x oil immersion; four interchangeable fluorescent/LED slots; and, in addition to fluorescence imaging, imaging modes for brightfield, digital color brightfield, phase contrast, and high contrast brightfield. Both two and four slide holders are available to customize throughput. The 4-slide holder is limited to objectives up to 40x when imaging coverslip down, and up to 20x when imaging coverslip up, due to the shorter working distance of higher magnification objectives. To automate uninterrupted high-throughput workflows, an Agilent BioTek BioStack 4 robotic arm can be integrated with an Agilent

BioTek Cytation 5 or Agilent BioTek Cytation 1 cell imaging multimode reader with many of the same features as the Agilent BioTek Lionheart FX, except for oil immersion. When considering instrument configuration options, a 4x objective may be useful for slide scanning to find imaging regions of interest more quickly.

## References

1. World Health Organization (WHO). 2015. Implementing Tuberculosis Diagnostics: Policy Framework. ISBN:978 92 4 150861 2. [https://www.who.int/tb/publications/implementing\\_TB\\_diagnostics/en](https://www.who.int/tb/publications/implementing_TB_diagnostics/en)
2. Mycobacteriology Laboratory Manual. 2014. The Global Laboratory Initiative, a Working Group of the Stop TB Partnership. <http://www.who.int/tb/laboratory/mycobacteriology-laboratory-manual.pdf>
3. Laboratory Diagnosis of Tuberculosis by Sputum Microscopy: The Handbook, Global edition. 2013. The Global Laboratory Initiative, a Working Group of the Stop TB Partnership. Published by SA Pathology. ISBN: 978-1-74243-602-9. [http://www.stoptb.org/wg/gli/assets/documents/TB%20MICROSCOPY%20HANDBOOK\\_FINAL.pdf](http://www.stoptb.org/wg/gli/assets/documents/TB%20MICROSCOPY%20HANDBOOK_FINAL.pdf)
4. Velayati, A. A.; Farnia, P. 2012. Morphological Characterization of Mycobacterium tuberculosis. DOI: 10.5772/29644. <https://www.intechopen.com/books/understanding-tuberculosis-deciphering-the-secret-life-of-the-bacilli/morphological-characteristic-of-mycobacterium-tuberculosis>
5. AFB Smear Microscopy. Association of Public Health Laboratories. [https://www.aphl.org/programs/infectious\\_disease/tuberculosis/TBCore/TB\\_AFB\\_Smear\\_Microscopy\\_TrainerNotes.pdf](https://www.aphl.org/programs/infectious_disease/tuberculosis/TBCore/TB_AFB_Smear_Microscopy_TrainerNotes.pdf)
6. Ridderhof, J. DrPH; Humes, R. MS, MT(ASCP)SM; and Boulahbal, F. External Quality Assessment for AFB Smear Microscopy. Joint publication. [https://www.aphl.org/aboutAPHL/publications/Documents/External\\_Quality\\_Assessment\\_for\\_AFB\\_Smear\\_Microscopy.pdf](https://www.aphl.org/aboutAPHL/publications/Documents/External_Quality_Assessment_for_AFB_Smear_Microscopy.pdf)
7. Mangels, J. I. *et al.* Methanol Fixation an Alternative to Heat Fixation of Smears Before Staining. *Diagnostic Microbiology and Infectious Disease* **1984**, 2(2), 129–137.
8. Minnerath, J. M. *et al.* A Comparison of Heat Versus Methanol Fixation for Gram Staining Bacteria. *Bioscene: Journal of College Biology Teaching* **2009**, 25(2), 36–41.

[www.agilent.com/lifesciences/biotek](http://www.agilent.com/lifesciences/biotek)

For Research Use Only. Not for use in diagnostic procedures.

RA44224.2268518519

This information is subject to change without notice.

© Agilent Technologies, Inc. 2019, 2021  
Printed in the USA, February 1, 2021  
5994-2546EN